Crystal structures of murine thrombin in complex with the extracellular fragments of murine protease-activated receptors PAR3 and PAR4

Alaji Bah, Zhiwei Chen, Leslie A. Bush-Pelc, F. Scott Mathews, and Enrico Di Cera*

Department of Biochemistry and Molecular Biophysics, Washington University School of Medicine, Box 8231, St. Louis, MO 63110

Edited by Russell F. Doolittle, University of California at San Diego, La Jolla, CA, and approved June 4, 2007 (received for review May 10, 2007)

It has been proposed that the cleaved form of protease-activated receptor 3 (PAR3) acts as a cofactor for thrombin cleavage and activation of PAR4 on murine platelets, but the molecular basis of this physiologically important effect remains elusive. X-ray crystal structures of murine thrombin bound to extracellular fragments of the murine receptors PAR3 (^{38}SFNGGPQNTFEEFPLSDIE^{56}) and PAR4 (^{51}KSSDKPNPR ↓ GYPGKFCANDSDTLELPASSQA^{81}, ↓ = site of cleavage) have been solved at 2.0 and 3.5 Å resolution, respectively. The cleaved form of PAR3, traced in the electron density maps from Gln-44 to Glu-56, makes extensive hydrophobic and electrostatic contacts with exosite I of thrombin through the fragment ^{47}FEEFPLSDIE^{56}. Occupancy of exosite I by PAR3 allosterically changes the conformation of the 60-loop and shifts the position of Trp-60d ≈10 Å with a resulting widening of the access to the active site. The PAR4 fragment, traced entirely in the electron density maps except for five C-terminal residues, clamps Trp-60d, Tyr-60a, and the aryl-binding site of thrombin with Pro-56 and Pro-58 at the P2 and P4 positions and engages the primary specificity pocket with Arg-59. The fragment then leaves the active site with Gly-60 and folds into a short helical turn that directs the backbone away from exosite I and over the autolysis loop. The structures demonstrate that thrombin activation of PAR4 may occur with exosite I available to bind cofactor molecules, like the cleaved form of PAR3, whose function is to promote substrate diffusion into the active site by allosterically changing the conformation of the 60-loop.

signal transduction | x-ray structure | allostery

Thrombin is an allosterically regulated serine protease that plays procoagulant, anticoagulant, and prothrombotic functions in the blood (1, 2). As a procoagulant factor, thrombin converts fibrinogen into an insoluble fibrin clot that anchors platelets to the site of lesion and initiates processes of wound repair. This action is reinforced and amplified by activation of the transglutaminase factor XIII that covalently stabilizes the fibrin clot and the proteolytic activation of factors V, VIII, and XI (3). In contrast, thrombin acts as an anticoagulant factor when it activates protein C. This function unfolds upon binding to thrombomodulin, a receptor on the membrane of endothelial cells, which suppresses the ability of thrombin to bind fibrinogen but enhances >1,000-fold the specificity of the enzyme toward the zymogen protein C. Activated protein C cleaves and inactivates factors Va and VIIIa, two essential cofactors of coagulation factors Xa and IXa that are required for thrombin generation, thereby down-regulating both the amplification and progression of the coagulation cascade (4). The prothrombotic role of thrombin depends mainly on cleavage of protease-activated receptors (PARs), which are members of the G protein-coupled receptor superfamily (5, 6). Four PARs have been cloned, and they all share the same basic mechanism of activation: thrombin and other proteases derived from the circulation and inflammatory cells cleave at a specific site within the extracellular N terminus to expose a new N-terminal tethered ligand domain, which binds intramolecularly and activates the cleaved receptor (6). Thrombin activates PAR1 (7), PAR3 (8, 9), and PAR4 (10–12) in this manner. Human platelets express PAR1 and PAR4, which mediate signaling and aggregation at low and high thrombin concentrations, respectively, and with distinct temporal characteristics (13). By contrast, murine platelets express PAR3 and PAR4. Upon cleavage by thrombin, PAR3, rather than itself mediating transmembrane signaling, functions as a cofactor that supports cleavage and activation of PAR4 at low thrombin concentrations (10, 11). On endothelial cells, PAR3 assists activation of PAR1 by promoting receptor heterodimerization (14).

An important feature of thrombin, also present in other clotting proteases, is to use extended exosites for recognition of physiologic substrates and cofactors (15–17). Exosites are spatially separated from the active-site region but linked to it by allosteric communication (2, 18–23). Exosite I occupies a position homologous to the Ca^{2+}-binding loop of trypsin and chymotrypsin (16, 24), 20–25 Å away from the active-site moiety, and is a binding epitope for fibrinogen (25–28), thrombomodulin (25, 29–32), and the thrombin receptors PAR1 (7, 26, 33, 34) and PAR3 (8, 26). The potent natural inhibitor hirudin also targets exosite I through its extended, acidic C-terminal domain (35). A hirudin-like acidic domain is present in PAR1 and PAR3 immediately downstream from the tethered ligand domain and has been invoked in the ability of these receptors to engage exosite I of thrombin (7, 10). Recognition of PAR4 is less dependent on exosite binding and relies almost entirely on the active-site moiety (26), especially through a pair of Pro residues at the P2 and P4 positions (36, 37). In addition, PAR4 constructs carrying a hirudin-like acidic domain fail to produce enhanced binding or catalytic processing (37), suggesting that PAR4 folds into a conformation unable to bind to exosite I.

The cofactor function of PAR3 on PAR4 cleavage and activation by thrombin in murine platelets (10, 11) implies binding of both PAR4 and the cleaved form of PAR3 to thrombin to form a ternary complex. After cleavage of PAR3, thrombin would remain bound to the receptor by means of exosite I. This complex would then engage PAR4 for proteolytic activation optimized by an allosteric effect of PAR3 bound to exosite I on the active-site moiety. A similar mechanism likely exists in human platelets where PAR4 can be cofactored by other receptors (10). In this work, we report the crystal structures of murine thrombin bound to extracellular fragments of murine

BIOCHEMISTRY

Author contributions: A.B. and E.D.C. designed research; A.B. and Z.C. performed research; L.A.B.-P. contributed new reagents/analytic tools; A.B., Z.C., F.S.M., and E.D.C. analyzed data; and E.D.C. wrote the paper.

The authors declare no conflict of interest.

This article is a PNAS Direct Submission.

Abbreviation: PAR, protease-activated receptor.

Data deposition: The atomic coordinates and structure factors have been deposited in the Protein Data Bank, www.pdb.org [PDB ID codes 2PUX (thrombin–PAR3 complex) and 2PV9 (thrombin–PAR4 complex)].

*To whom correspondence should be addressed. E-mail: enrico@wustl.edu.

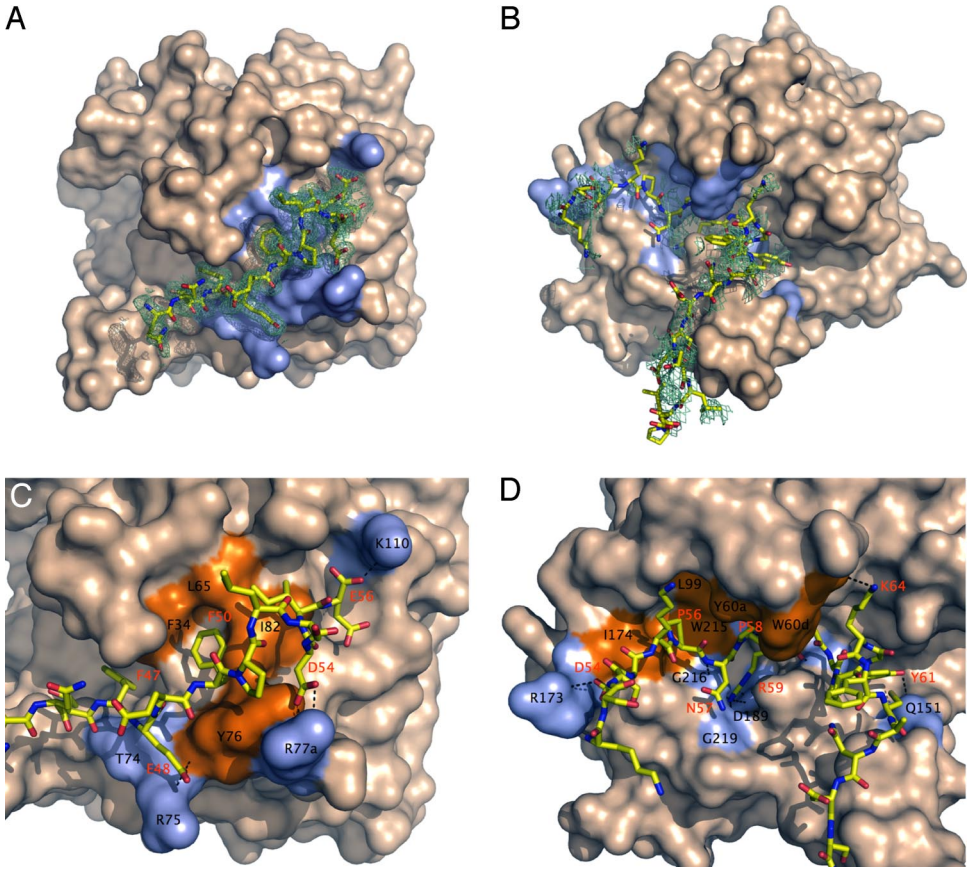

Fig. 1. Structures of murine thrombin in complex with fragments of murine PAR3 (*A* and *C*) and PAR4 (*B* and *D*). (*A* and *B*) Thrombin is rendered in surface representation (wheat) with the residues <4 Å from the bound fragment of PAR3 or PAR4 (stick model) colored in light blue. The orientation is centered on exosite I (*A*) or the active site (*B*). The orientation in *A* is obtained from *B* by ≈90° rotation along the *y* axis. Electron density maps (green mesh) are contoured at 1.0 (*B*) or 0.7 (*D*) σ. (*C* and *D*) Details of the molecular contacts at the thrombin–PAR interface, with hydrophobic regions of the thrombin epitope colored in orange and polar regions colored in light blue. H-bonds are depicted as broken lines. Residues involved in contacts <4 Å are listed in Table 1 and are labeled in black for thrombin and red for PAR. (*C*) The cleaved fragment of PAR3 engages exosite I through polar and hydrophobic interactions. (*D*) The fragment of PAR4 comprising the scissile bond makes extensive interactions with the active-site moiety of the enzyme by using the Pro-56 and Pro-58 clamp at the P2 and P4 positions. After exiting the active site, the fragment folds into a short helical turn and is deflected away from exosite I and to the autolysis loop right below the active-site region.

PAR3 and PAR4. The structures reveal the molecular basis of the cofactor function of cleaved PAR3, bound to exosite I, on recognition of PAR4 by the active site of thrombin.

Results

Murine thrombin inactivated with the single-site mutation S195A was crystallized in complex with the extracellular fragment of murine PAR3, ^{38}SFNGGPQNTFEEFPLSDIE^{56}, corresponding to the sequence downstream from the cleavage site at Lys-37 and containing the hirudin-like motif ^{47}FEEFP^{51} predicted to bind to exosite I (11, 37). Although the structure was solved at relatively high resolution (2.0 Å), only the sequence ^{44}QNTFEEFPLSDIE^{56} of the extracellular fragment of PAR3 could be detected in the electron density maps. Density for the sequence ^{38}SFNGGP^{43} was too weak to allow for conclusive assignments. The PAR3 fragment engages exosite I of murine thrombin in a number of well defined interactions starting with Phe-47 (Fig. 1 *A* and *C* and Table 1). The three residues ^{44}QNT^{46} fold away from the thrombin surface, as seen in the NMR structure of a cleaved fragment of PAR1 (38). The aromatic ring of Phe-47 is edge-to-face with the aromatic ring of Phe-34 of thrombin. On the opposite side of Phe-34 lies the side chain of Phe-50, also oriented perpendicular to the benzene ring of the thrombin residue. Phe-50 is at the center of a hydrophobic cluster that includes Leu-52 and Ile-55 of PAR3 in van der Waals interactions. The cluster docks on an extended hydrophobic patch of exosite I comprising Phe-34, Leu-65, Tyr-76, and Ile-82. In addition to the substantial hydrophobic contacts at the thrombin–PAR3 interface, the complex is stabilized by electrostatic and polar interactions. The backbone N atom of Glu-48 engages the backbone O atom of Thr-74 of thrombin and the Oε1 atom forms an ion pair with the Nε atom of Arg-75 and an H-bond with the backbone N atom of Tyr-76 of thrombin. Asp-54 uses its carboxylate oxygens to contact Arg-77a of thrombin through the NH2 and Nε atoms. Finally, Glu-56 engages the Nζ atom of Lys-110 of thrombin by means of its C-terminal carboxylate atoms and H-bonds to the O atom of Ile-82 through its N atom. Overall, the surface of interaction between thrombin and PAR3 is composed of a hydrophobic patch surrounded by a periphery of polar/electrostatic contacts. The interactions involve the hirudin-like motif ^{47}FEEFP^{51} predicted to bind to exosite I (11, 37) but also the sequence ^{52}LSDIE^{56} that internally stabilizes the fold of the bound PAR3 and provides additional polar contacts with the thrombin surface.

The structure of murine thrombin in the free form has been solved recently (39). Comparison with the structure of the murine thrombin–PAR3 complex (Table 2) reported here reveals an

Table 1. Interatomic contacts (<4 Å) between thrombin, PAR3, and PAR4

Thrombin	PAR3	PAR4	Distance, Å
Phe-34	Phe-47		vdW*
Thr-74 O	Glu-48 N		2.90
Arg-75 Nε	Glu-48 Oε1		3.02
Tyr-76 N	Glu-48 Oε1		2.65
Phe-34, Leu-65, Tyr-76, Ile-82	Phe-50		vdW
Arg-77a Nε	Asp-54 Oδ1		3.10
Arg-77a NH2	Asp-54 Oδ2		3.47
Ile-82 O	Glu-56 N		2.82
Lys-110 Nζ	Glu-56 OT		3.19
Arg-173 NH1		Asp-54 Oδ1	3.66
Leu-99, Ile-174, Trp-215		Pro-56	vdW
Gly-216 O		Asn-57 N	3.37
Gly-216 N		Asn-57 O	3.22
His-57, Tyr-60a, Trp-60d		Pro-58	vdW
Asp-189 Oδ1		Arg-59 NH1	3.63
Ala-190 O		Arg-59 NH1	2.27
Gly-216 O		Arg-59 NH2	3.77
Gly-219 O		Arg-59 NH2	2.84
Asp-189 Oδ2		Arg-59 NH2	3.66
Ser-214 O		Arg-59 N	3.29
Gly-193 N		Arg-59 O	2.22
Gln-151 Nε2		Tyr-61 OH	3.52
Trp-60d O		Lys-64 Nζ	3.96

*vdW, van der Waals contact.

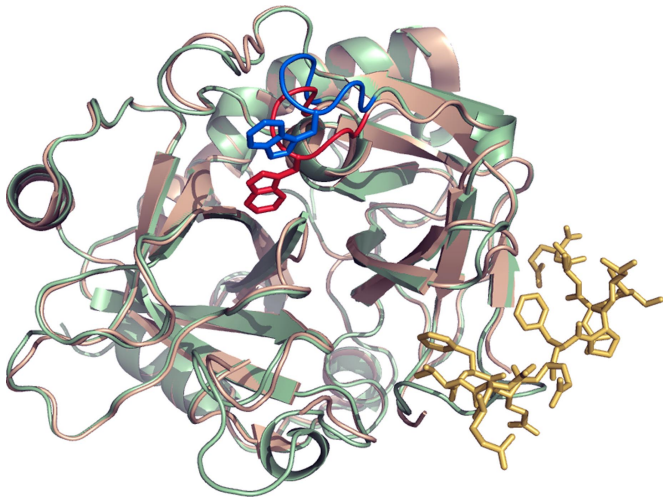

Fig. 2. Allosteric effect induced by binding of the cleaved fragment of murine PAR3 (stick model in gold) to exosite I of murine thrombin (ribbon model in light green) on the conformation of the 60-loop (blue) and the position of Trp-60d. Comparison with the free structure of murine thrombin (ribbon model in wheat, with 60-loop and Trp-60d in red) shows a significant upward shift of the ^{60a}YPPWDK^{60f} region of the 60-loop and a 180° flip of the indole ring of Trp-60d. The change produces complete aperture of the active site to facilitate substrate diffusion. The allosteric communication between exosite I and the 60-loop documented in the thrombin–PAR3 structure may be relevant to the interaction of thrombin with other exosite I ligands, such as thrombomodulin.

enzyme conformation that is largely unmodified except for one notable feature. The presence of PAR3 bound to exosite I causes a rearrangement of the 60-loop lining the upper rim of the active-site entrance (Fig. 2). In the free enzyme and in human thrombin (40, 41), the indole ring of Trp-60d partially occludes access to the active site and restricts specificity toward physiologic substrates and inhibitors (15). When PAR3 binds to exosite I, the 60-loop shifts 3.8 Å upward and causes a 180° flip of Trp-60d around the Cβ≡Cγ bond that projects the indole ring into the solvent and opens up the active site fully. It is well known that binding of the C-terminal acidic tail of hirudin (hirugen) to exosite I elicits allosteric effects on the active site of thrombin (18, 21), but structural evidence of this communication has remained elusive. Interestingly, cleaved PAR3 binds to exosite I of murine thrombin in a conformation almost identical to that determined for hirugen bound to exosite I of the human enzyme (42). The conformation and molecular contacts of the hirudin-like motif ^{47}FEEFP^{51} are practically identical to those of the sequence ^{56}FEEIP^{60} of hirugen. Yet, binding of hirugen has minimal effects on the position of the 60-loop of thrombin, and Trp-60d retains an orientation that partially occludes the active-site cleft and screens the catalytic His-57 from solvent (42). On the other hand, the structure of murine thrombin bound to cleaved PAR3 at exosite I reveals the basis of the allosteric communication between exosite I and the active-site cleft. Key to this allosteric effect is the ability of Trp-60d to move like a flap and regulate substrate diffusion into the active site. The structural flexibility documented for this and other Trp residues of thrombin is in agreement with recent spectroscopic measurements (43).

Murine thrombin mutant S195A was also crystallized in complex with the extracellular fragment of murine PAR4, ^{51}KSSDKPNPR↓GYPGKFCANDSDTLELPASSQA^{81} (↓ = site of cleavage), containing the cleavage site at Arg-59. Although the structure was solved at low resolution (3.5 Å), 26 residues of the fragment from Lys-51 to Pro-76 could be traced in the electron density maps. Overall, the thrombin conformation is similar to that seen in the thrombin–PAR3 complex (rmsd 0.524 Å), but Trp-60d retains its canonical orientation with the indole ring pointing down over the active site (Fig. 1 *B* and *D*) in contact with PAR4. Of great importance are the contacts made by PAR4 with the active site of thrombin (Fig. 1 *B* and *D* and Table 1). Arg-59 penetrates the primary specificity pocket and engages several residues. The guanidinium group makes a strong bidentate ion pair with the carboxylate oxygens of Asp-189 and three H-bonds with the backbone O atoms of Gly-216, Gly-219, and Ala-190. The backbone O atom of Arg-59 makes a short H-bond with the N atom of Gly-193 in the oxyanion hole, and the backbone N atom H-bonds to the backbone O atom of Ser-214. These are the canonical interactions expected for Arg of substrate in the specificity pocket of a trypsin-like protease (16, 44, 45). Extensive interactions are also present away from the primary specificity pocket. Pro-58 at the P2 position of substrate makes numerous van der Waals contacts with the catalytic His-57, Tyr-60a, and Trp-60d in the 60-loop. Its backbone O atom could experience electrostatic repulsion from the Oε2 atom of Glu-192 that is 3.4 Å away. The P3 residue Asn-57 points away from the thrombin surface with its side chain, as expected for an amino acid in the L-enantiomer at this position (40), but its backbone N and O atoms H-bond to the O and N atoms of Gly-216 again in compliance with the canonical antiparallel mode of interaction of substrate with the active site of serine proteases (16, 44, 45). The P4 residue Pro-56 makes numerous van der Waals interactions with the aryl-binding site composed of Leu-99, Ile-174, and Trp-215 with which it makes a strong edge-to-face interaction similar to that seen for the H-D-Phe residue of the inhibitor H-D-Phe-Pro-Arg-CH_2Cl (40, 41). Together, Pro-56 and Pro-58 produce a clamp that latches PAR4 onto the active site of thrombin by using a large hydrophobic surface from the aryl-binding site on one side and the 60-loop on the opposite side of the catalytic His-57. The conformation of the ^{56}PNPR^{59} sequence of PAR4 is practically identical to that predicted by NMR studies of the human PAR4 sequence ^{44}PAPR^{47} (36) and supports the critical role of this Pro

BIOCHEMISTRY

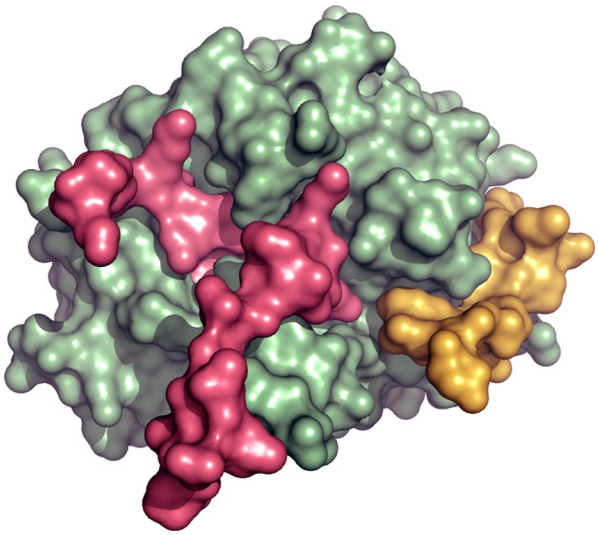

Fig. 3. Putative ternary complex of thrombin, cleaved PAR3 and PAR4 derived from an overlay of the crystal structures of the murine thrombin–PAR4 and thrombin–PAR3 complexes. Thrombin (green) refers to the thrombin–PAR4 complex. Binding of cleaved PAR3 (gold) to exosite I does not interfere with binding of PAR4 (red) to the active site of the enzyme. Cleaved PAR3 may therefore act as a cofactor of PAR4 cleavage by thrombin.

pair in thrombin recognition uncovered by functional studies (37). The P5 residue Lys-55 leaves the active-site moiety, although a slight conformational change could put it in electrostatic coupling with Glu-97a of thrombin. Upstream from Lys-55, Asp-54 at P6 makes a long H-bond with the guanidinium group of Arg-173 before the rest of the PAR4 peptide leaves the thrombin surface.

Downstream from the scissile bond, the P1′ residue Gly-60 initiates a turn followed by a short helical segment stabilized by an H-bond between the O atom of Pro-62 and the N atom of Cys-66. The helix turn is an intrinsic property of PAR4 because the conformation of the fragment in this region is not influenced by any packing interactions with symmetry-related molecules. Without Pro-62, the fragment of PAR4 would likely pursue the 30-loop and exosite I of thrombin. The helix turn stabilizes and redirects PAR4 toward the autolysis loop right below the entrance to the active site. The P2′ residue Tyr-61 positions its OH atom within H-bonding distance of the Nε2 atom of Gln-151, but its aromatic ring is too far from any stabilizing interaction with Leu-40 of thrombin. The P5′ residue Lys-64 contacts the backbone O atom of Trp-60d with its Nζ atom, but a slight rearrangement could bring it in favorable electrostatic coupling with the carboxylate group of Asp-60e and facilitate a stacking interaction of Phe-65 with Trp-60d of thrombin. Of the remaining residues on the C terminus of the PAR4 fragment, none makes specific interactions with the autolysis loop of thrombin whose residues Trp-148 and Thr-149a lie right below Cys-66 and Ser-70 of PAR4. The mode of interaction of PAR4 with thrombin calls for numerous interactions with the active site and the aryl-binding site, leaving exosite I and the 30-loop free. Cleavage of PAR4 does not require binding to exosite I of thrombin, in agreement with earlier mutagenesis studies (11, 37). The structured helix of PAR4 makes it difficult to predict whether introduction of a hirudin-like sequence downstream from the scissile bond would confer affinity toward exosite I. Contrasting results have been reported in this connection (11, 37). If the helix remains rigid, the backbone downstream from Cys-66 should be directed toward the autolysis loop and not exosite I. However, insertion of a properly spaced hirudin-like sequence could endow PAR4 with exosite I binding by unraveling the helix turn.

Table 2. Crystallographic data for the murine thrombin–PAR complexes

Parameter	PAR3 (2PUX)	PAR4 (2PV9)
Data collection		
Wavelength, Å	0.9	1.54
Space group	C2	P6(5)22
Unit cell dimension, Å	a = 146.0	a = 111.2
	b = 48.2	b = 111.2
	c = 62.0	c = 179.7
	β = 106.2°	
Molecules/asymmetric unit	1	1
Resolution range, Å	40.0–2.0	40.0–3.5
Observations	97,904	73,773
Unique observations	27,610	8,568
Completeness, %	97.2 (88.6)	97.1 (86.3)
R_{sym}, %	10.0 (30.6)	11.0 (32.8)
$I/\sigma(I)$	10.6 (2.9)	11.2 (2.3)
Refinement		
Resolution, Å	40.0–2.0	40.0–3.5
$F/\sigma(\|F\|)$	>0	>0
R_{cryst}, R_{free}	0.185, 0.225	0.306, 0.319
Reflections (working/test)	24,671/1,238	8,080/472
Protein atoms	2,578	2,680
Solvent molecules	295	0
rmsd bond lengths*, Å	0.011	0.010
rmsd angles*,°	1.6	1.8
rmsd ΔB, Å²; mm/ms/ss†	2.39/3.00/3.94	–/–/–
$<B>$ protein, Å²	20.8	42.5
$<B>$ solvent, Å²	32.3	—
Ramachandran plot		
Most favored, %	99.3	95.7
Generously allowed, %	0.7	3.9
Disallowed, %	0.0	0.4

*Root mean square deviation (rmsd) from ideal bond lengths and angles and rmsd in B factors of bonded atoms.

†mm, main chain–main chain; ms, main chain–side chain; ss, side chain–side chain.

Finally, the presence of the short helical turn includes residues of the tethered ligand domain ^{60}GYPGKF^{65} (10–12) and suggests that the activation peptide may bind to the receptor by using a structured conformation rather than an extended sheet.

Discussion

An obvious conclusion can be drawn from the structures presented in this work. The cleaved form of PAR3 bound to exosite I, as shown in Fig. 1 *A* and *C*, does not interfere with binding of the intact PAR4 to thrombin, as shown in Fig. 1 *B* and *D*. The cleaved PAR3 and intact PAR4 fragments bind to thrombin without overlap and can generate a ternary complex where PAR3 functions as a cofactor that allosterically optimizes PAR4 cleavage (Fig. 3).

The role of exosite I as a locale for cofactor binding to thrombin is well documented. A number of peptides targeting exosite I influence allosterically the active site of thrombin and bring about significant changes in activity and even substrate specificity (18–21, 46). On the surface of platelets, the cofactor role of PAR3 may exploit the allosteric communication between exosite I and the active site or simply manifest itself as a favorable anchoring of thrombin that reduces the cost of diffusion when PAR4 is targeted for cleavage. The structure of thrombin bound to PAR3 reveals a snapshot of the mechanism for the allosteric communication in terms of a shift in the indole ring of Trp-60d and upward movement of the entire 60-loop that open up the active-site cleft. That facilitates substrate diffusion into the active site and enhances k_{cat}/K_m values for hydrolysis (18). A similar mechanism may exist

upon thrombomodulin binding to thrombin because the large change in specificity elicited toward protein C is the result of enhanced substrate diffusion into the active site (32). The structure of thrombin bound to a fragment of thrombomodulin in exosite I does not document changes in accessibility of the active site (30). However, the structure contains an inhibitor in the active site that likely abrogates any rearrangement in the 60-loop induced upon exosite I binding. The presence of active-site inhibitors is known to abrogate large structural changes affecting the active site (47). The structure of murine thrombin bound to cleaved PAR3 refutes a long-held assumption on the rigidity of the 60-loop (40), which was first called into question by the structure of the thrombin mutant E192Q bound to the Kunitz inhibitor BPTI that forced its way into the active site of the enzyme (48). This finding documented a significant departure from the modest mobility seen in previous structures (42, 49). The structure of the thrombin–PAR3 complex offers convincing evidence that the position of Trp-60d and the 60-loop can be modified allosterically by binding to exosite I when the active site of thrombin is free. This finding has far-reaching consequences on our understanding of the molecular underpinnings of other allosteric transitions of thrombin, such as those linked to thrombomodulin and Na^+ binding (2, 15, 41).

Materials and Methods

The murine thrombin mutant S195A was constructed, expressed, and purified to homogeneity as described previously (50). Soluble fragments of murine PAR3 and PAR4 corresponding to the extracellular portions of the receptors were synthesized by solid phase, purified to homogeneity by HPLC, and tested for purity by mass spectrometry. Their sequences are ^{38}SFNGGPQNTFEEFPLSDIE^{56} for the cleaved form of PAR3 and ^{51}KSSDKPNPR ↓ GYPGKFCANDSDTLELPASSQA^{81} for PAR4 (↓ = site of cleavage).

The enzyme solution for crystallization screens was prepared by concentrating 4 ml of 0.77 mg/ml S195A murine thrombin to 7.7 mg/ml in buffer Q (50 mM choline chloride/20 mM Tris, pH 7.4) by using a Centricon YM10 filter (Millipore, Bedford, MA). Solutions of PAR3 and PAR4 were prepared in the same buffer Q to an 18.8 and 14 mM final concentration, respectively. Thrombin–PAR complexes were generated by mixing the S195A mutant and PAR solutions at a 1:11 molar ratio, and they were incubated at room temperature for 1 h. We found no evidence of cleavage of the PAR fragments by the S195A mutant. Initial crystal screenings were performed with the PEG Suite (Qiagen, Valencia, CA). Vapor diffusion with hanging drops was used to generate crystals. For each of the 96 screen conditions, a hanging drop was prepared by mixing 1 μl of thrombin–PAR complex and 1 μl of reservoir solution, and the drop was allowed to equilibrate with 1 ml of crystallization buffer at 23°C. Crystals started to grow within 4 days for the thrombin–PAR4 complex and 6 days for the thrombin–PAR3 complex. The best crystallization condition for the thrombin–PAR4 complex was obtained in 20% PEG 3350 and 200 mM $MgSO_4(H_2O)_7$ and was optimized by using 16–24% PEG 3350 and 140–260 mM $MgSO_4(H_2O)_7$. Crystals of the thrombin–PAR3 complex grew initially in 20% PEG 10,000 and 0.1 M Hepes (pH 7.5). Optimization was performed by using 16–24% PEG 10,000 and 0.04–0.16 M Hepes (pH 7.5). Crystals were allowed to grow for 10 days before they were cryoprotected in crystallization buffer containing 15% glycerol and then flash-frozen in liquid N_2. Crystallization of the ternary complex thrombin–PAR3–PAR4 was unsuccessful.

X-ray diffraction data for the crystal of the thrombin–PAR4 complex were collected in house on a RAXIS IV detector (Rigaku/MSC, The Woodlands, TX). Data for the thrombin–PAR3 crystal were collected on an ADSC Quantum 315 CCD detector at the Biocars Beamline 14-BM-C of Advanced Photon Source, Argonne National Laboratories (Argonne, IL). Unfortunately, crystals of the thrombin–PAR4 complex diffracted poorly at the Biocars Beamline with no improvement in resolution compared with the data collected in house. The space group was C2 for the thrombin–PAR3 complex and P6 (5)22 for the thrombin–PAR4 complex, with unit cell dimensions listed in Table 2. Both complexes crystallized with a single molecule in the asymmetric unit. Reflection data were indexed, integrated, and scaled by using the HKL2000 software package (51). Both structures were solved by molecular replacement with MOLREP from the CCP4 package (52) by using the coordinates of the PPACK-inhibited form of human thrombin [Protein Data Bank (PDB) ID code 1SHH] (41) as a starting model. Refinement and electron density generation were performed with Crystallography and NMR System (CNS) software package (53), and 5% of the reflections were randomly selected as a test set for cross-validation. Ramachandran plots were calculated by using PROCHECK (54). Results of data processing and refinement are summarized in Table 2. Coordinates of the structures of murine thrombin in complex with fragments of murine PAR3 and PAR4 have been deposited to the Protein Data Bank (accession codes: 2PUX for the thrombin-PAR3 complex and 2PV9 for the thrombin-PAR4 complex).

This work was supported in part by the National Institutes of Health Research Grants HL49413, HL58141, and HL73813 (to E.D.C.).

1. Di Cera E (2003) *Chest* 124:11S–17S.
2. Di Cera E, Page MJ, Bah A, Bush-Pelc LA, Garvey LC (2007) *Phys Chem Chem Phys* 9:1292–1306.
3. Davie EW, Kulman JD (2006) *Semin Thromb Hemostasis* 32(Suppl 1):3–15.
4. Esmon CT (2003) *Chest* 124:26S–32S.
5. Brass LF (2003) *Chest* 124:18S–25S.
6. Coughlin SR (2000) *Nature* 407:258–264.
7. Vu TK, Wheaton VI, Hung DT, Charo I, Coughlin SR (1991) *Nature* 353:674–677.
8. Ishihara H, Connolly AJ, Zeng D, Kahn ML, Zheng YW, Timmons C, Tram T, Coughlin SR (1997) *Nature* 386:502–506.
9. Sambrano GR, Weiss EJ, Zheng YW, Huang W, Coughlin SR (2001) *Nature* 413:74–78.
10. Kahn ML, Zheng YW, Huang W, Bigornia V, Zeng D, Moff S, Farese RV, Jr, Tam C, Coughlin SR (1998) *Nature* 394:690–694.
11. Nakanishi-Matsui M, Zheng YW, Sulciner DJ, Weiss EJ, Ludeman MJ, Coughlin SR (2000) *Nature* 404:609–613.
12. Xu WF, Andersen H, Whitmore TE, Presnell SR, Yee DP, Ching A, Gilbert T, Davie EW, Foster DC (1998) *Proc Natl Acad Sci USA* 95:6642–6646.
13. Shapiro MJ, Weiss EJ, Faruqi TR, Coughlin SR (2000) *J Biol Chem* 275:25216–25221.
14. McLaughlin JN, Patterson MM, Malik AB (2007) *Proc Natl Acad Sci USA* 104:5662–5667.
15. Bode W (2006) *Blood Cells Mol Dis* 36:122–130.
16. Page MJ, MacGillivray RTA, Di Cera E (2005) *J Thromb Haemostasis* 3:2401–2408.
17. Fenton JW, II (1986) *Ann NY Acad Sci* 485:5–15.
18. Ayala Y, Di Cera E (1994) *J Mol Biol* 235:733–746.
19. Lai MT, Di Cera E, Shafer JA (1997) *J Biol Chem* 272:30275–30282.
20. Liu LW, Vu TK, Esmon CT, Coughlin SR (1991) *J Biol Chem* 266:16977–16980.
21. Vindigni A, White CE, Komives EA, Di Cera E (1997) *Biochemistry* 36:6674–6681.
22. Verhamme IM, Olson ST, Tollefsen DM, Bock PE (2002) *J Biol Chem* 277:6788–6798.
23. Colwell NS, Blinder MA, Tsiang M, Gibbs CS, Bock PE, Tollefsen DM (1998) *Biochemistry* 37:15057–15065.
24. Bartunik HD, Summers LJ, Bartsch HH (1989) *J Mol Biol* 210:813–828.
25. Tsiang M, Jain AK, Dunn KE, Rojas ME, Leung LL, Gibbs CS (1995) *J Biol Chem* 270:16854–16863.
26. Ayala YM, Cantwell AM, Rose T, Bush LA, Arosio D, Di Cera E (2001) *Proteins* 45:107–116.
27. Pechik I, Madrazo J, Mosesson MW, Hernandez I, Gilliland GL, Medved L (2004) *Proc Natl Acad Sci USA* 101:2718–2723.
28. Pechik I, Yakovlev S, Mosesson MW, Gilliland GL, Medved L (2006) *Biochemistry* 45:3588–3597.
29. Hall SW, Nagashima M, Zhao L, Morser J, Leung LL (1999) *J Biol Chem* 274:25510–25516.
30. Fuentes-Prior P, Iwanaga Y, Huber R, Pagila R, Rumennik G, Seto M, Morser J, Light DR, Bode W (2000) *Nature* 404:518–525.

31. Pineda AO, Cantwell AM, Bush LA, Rose T, Di Cera E (2002) *J Biol Chem* 277:32015–32019.
32. Xu H, Bush LA, Pineda AO, Caccia S, Di Cera E (2005) *J Biol Chem* 280:7956–7961.
33. Myles T, Le Bonniec BF, Stone SR (2001) *Eur J Biochem* 268:70–77.
34. Mathews II, Padmanabhan KP, Ganesh V, Tulinsky A, Ishii M, Chen J, Turck CW, Coughlin SR, Fenton JW, II (1994) *Biochemistry* 33:3266–3279.
35. Rydel TJ, Tulinsky A, Bode W, Huber R (1991) *J Mol Biol* 221:583–601.
36. Cleary DB, Trumbo TA, Maurer MC (2002) *Arch Biochem Biophys* 403:179–188.
37. Jacques SL, Kuliopulos A (2003) *Biochem J* 376:733–740.
38. Seeley S, Covic L, Jacques SL, Sudmeier J, Baleja JD, Kuliopulos A (2003) *Chem Biol* 10:1033–1041.
39. Marino F, Chen ZW, Ergenekan C, Bush-Pelc LA, Mathews FS, Di Cera E (2007) *J Biol Chem* 282:16355–16361.
40. Bode W, Turk D, Karshikov A (1992) *Protein Sci* 1:426–471.
41. Pineda AO, Carrell CJ, Bush LA, Prasad S, Caccia S, Chen ZW, Mathews FS, Di Cera E (2004) *J Biol Chem* 279:31842–31853.
42. Vijayalakshmi J, Padmanabhan KP, Mann KG, Tulinsky A (1994) *Protein Sci* 3:2254–2271.
43. Bah A, Garvey LC, Ge J, Di Cera E (2006) *J Biol Chem* 281:40049–40056.
44. Hedstrom L (2002) *Chem Rev* 102:4501–4524.
45. Perona JJ, Craik CS (1995) *Protein Sci* 4:337–360.
46. Parry MA, Stone SR, Hofsteenge J, Jackman MP (1993) *Biochem J* 290:665–670.
47. Pineda AO, Chen ZW, Caccia S, Cantwell AM, Savvides SN, Waksman G, Mathews FS, Di Cera E (2004) *J Biol Chem* 279:39824–39828.
48. van de Locht A, Bode W, Huber R, Le Bonniec BF, Stone SR, Esmon CT, Stubbs MT (1997) *EMBO J* 16:2977–2984.
49. Malkowski MG, Martin PD, Guzik JC, Edwards BFP (1997) *Protein Sci* 6:1438–1448.
50. Bush LA, Nelson RW, Di Cera E (2006) *J Biol Chem* 281:7183–7188.
51. Otwinowski Z, Minor W (1997) *Methods Enzymol* 276:307–326.
52. Bailey S (1994) *Acta Crystallogr D* 50:760–763.
53. Brunger AT, Adams PD, Clore GM, DeLano WL, Gros P, Grosse-Kunstleve RW, Jiang JS, Kuszewski J, Nilges M, Pannu NS, *et al.* (1998) *Acta Crystallogr D* 54:905–921.
54. Morris AL, MacArthur MW, Hutchinson EG, Thornton JM (1992) *Proteins* 12:345–364.